Recommended Paper

A Smartphone 3D Positioning Method using a Spinning Magnet Marker

Kosuke Watanabe[1,a]   Kei Hiroi[2]   Takeshi Kamiyama[3]   Hiroyuki Sano[4]
Masakatsu Tsukamoto[5]   Masaji Katagiri[6]   Daizo Ikeda[4]   Katsuhiko Kaji[7]
Nobuo Kawaguchi[2]

Abstract: In recent years, the importance of location information has increased due to the popularization of terminals such as smartphones. Our purpose is to estimate the 3D position of smartphones within several centimeters. This location information can reveal a person's behavior patterns and subject of interest. A method based on dynamic magnetism can estimate the 3D position of a terminal within several centimeters, and it is robust against the environment. However, since the performance of the smartphone's magnetic sensor is limited, this method cannot be used in smartphones. In this research, we propose a smartphone 3D positioning method using a Spinning Magnet Marker (SMM) that spins a powerful neodymium magnet with a motor. Magnetoquasistatic field generated by an SMM is detected by a magnetic sensor mounted on a smartphone, and the 3D position of a smartphone based on the SMM is estimated from the magnetism. We developed an SMM with a stepper motor to improve estimation accuracy. In addition, we studied the magnetism generated by an SMM and derive equations to estimate the 3D position of a smartphone. Furthermore, we improved the estimation accuracy and expanded coverage by introducing a noise reduction method. We evaluate the estimation accuracy of the proposed method. When the azimuth angle is 0°, the elevation angle is 0°, and the distance is 3 m, the azimuth angle is estimated with a mean error of 1°, the elevation angle is estimated with a mean error of 4°, and the distance is estimated with a mean error of 9 cm.

Keywords: indoor positioning, smartphone, magnetism, three-dimension, magnetoquasistatic field

1. Introduction

In recent years, with the spread of terminals such as smartphones, various location-based services have increased. GPS (Global Positioning System) is often used to obtain location information outdoors. However, it is difficult to use GPS indoors where radio waves are difficult to reach. When the 3D position of a smartphone can be estimated within several centimeters, it is expected that it is possible to estimate the behavior patterns of people and the target of interest. For example, when you know the angle from which you are watching the exhibition at an event venue, you can recognize what are targets of visitor's interest. In addition, when it is possible to estimate the route of a visitor within an accuracy of several centimeters, it is possible to estimate the behavior pattern of visitors in detail. Various indoor positioning methods have been studied to date. For example, there are methods based on radio waves such as Wi-Fi access points [1], [2], [3], [4], BLE (Bluetooth Low Energy) [5], [6], [7], and UWB (Ultra Wide Band) technology [8]. However, in these methods, it is difficult to estimate the position of a terminal within several centimeters. In addition, estimation accuracy decreases when there is an obstacle between the transmitter and terminal. Other methods based on ultrasound [9], [10], [11], and VLP (Visual Light Positioning) [12], [13] can estimate a position within several centimeters. However, estimation accuracy decreases when an obstacle exists that is similar to the positioning method based on radio waves. Since smartphones are often carried in clothes and bags, these methods are not suitable for our purpose.

A positioning method based on dynamic magnetism [16], [17], [18], [19] has higher robustness than methods based on radio waves; magnetism has stronger permeability than radio waves. Actually, there are commercial products based on dynamic magnetism that track movement or positioning indoor locations. However, methods based on dynamic magnetism are subject to difficulties with smartphones. For example, these methods use dynamic magnetism at a frequency of several kilohertz. Since the sampling frequency of smartphone magnetic sensors is a few dozen hertz, it cannot detect magnetism that is several kilohertz.

[1] Graduate School of Engineering, Nagoya University, Nagoya, Aichi 464–0814, Japan
[2] Institutes of Innovation for Future Society, Nagoya University, Nagoya, Aichi 464–8601, Japan
[3] IoT Business Department, NTT DOCOMO, INC., Yokosuka, Kanagawa 239–8536, Japan
[4] Research Laboratories, NTT DOCOMO, INC., Yokosuka, Kanagawa 239–8536, Japan
[5] Product Department, NTT DOCOMO, INC., Yokosuka, Kanagawa 239–8536, Japan
[6] R&D Information Service Department, DOCOMO Technology, Inc., Yokosuka, Kanagawa 239–8536, Japan
[7] Faculty of Information Science, Aichi Institute of Technology, Toyota, Aichi 470–0392, Japan
[a] nabeko@ucl.nuee.nagoya-u.ac.jp

Fig. 1 Concept of 3D positioning using an SMM.

Table 1 Comparison with previous research using an SMM.

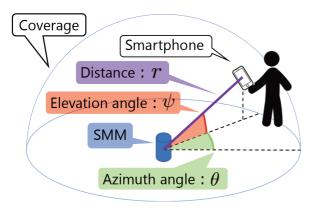|	Purpose	Accuracy (at $r = 2$ m, $\theta = 0°$, $\psi = 0°$)	Coverage
Previous Research (Refs. [21], [22])	Passengers Detection, Two-Dimensional Positioning	13 cm	2 m
This Research	3D Positioning	1 cm	3 m

In addition, because a current of several amperes is required to generate magnetism that can be detected by a smartphone's magnetic sensor from several meters away, methods based on coils with an electric current are not suitable.

In order to use the method based on the dynamic magnetism for smartphones, we developed a Spinning Magnet Marker (SMM). An SMM generates a magnetoquasistatic field by spinning a magnet and most smartphones include a magnetic sensor which can detect this magnetism. When an SMM is set at a specific position, the position of a smartphone with respect to the SMM can be estimated. Previously, we studied a method for detecting passengers with smartphones [20], [21] and a two-dimensional smartphone positioning method [22] using an SMM.

In this paper, we propose a smartphone 3D positioning method using an SMM. The proposed method can be used to estimate the 3D positions of several smartphones at the same time. We illustrate the concept of our proposal in **Fig. 1**. Throughout this paper, we denote the distance by "r", the azimuth angle by "θ", and the elevation angle by "ψ".

We have previously proposed a 3D positioning method for smartphones using an SMM [23]. The difference between this method and the previous method is that in the previous method, the distance r estimation was only applicable when the elevation angle was $\psi = 0°$, whereas in this method, by improving the distance estimation method, we are able to estimate distance r at arbitrary elevation angle ψ. Moreover, in previous research, we conducted experiments separately to evaluate the estimation accuracies of the azimuth angle θ, the elevation angle ψ, and the distance r. On the other hand, in this study, we conduct experiments simultaneously to evaluate the accuracy of the azimuth angle θ, the elevation angle ψ, and the distance r at each 3D position.

We explain the method to estimate the azimuth angle θ, the elevation angle ψ, and the distance r, and the procedure for improving estimation accuracy. We conducted experiments to estimate the azimuth angle θ, the elevation angle ψ, and the distance r separately as preliminary experiments. In addition, we conducted experiments to evaluate the estimation accuracies of the azimuth angle θ, elevation angle ψ, and distance r simultaneously at each 3D position of a smartphone.

Table 1 shows a comparison with our previous research [21], [22]. We have achieved improvements over our previous research in the following three respects. First, it is now possible to detect the 3D position of a smartphone. Second, we developed a new SMM and improved estimation accuracy. Third, we expanded coverage to 3 m by adding a procedure for reducing the effects from noise in magnetic data.

The first contribution is that the proposed method is a positioning method capable of detecting the position of a person to within a few centimeters. Incorporating this technology into smartphones allows application to a variety of scenes and situations. Location information service may be achieved not only for apparel products but also for stores such as bookstores and but also for most stores regardless of store type.

The second contribution is that the proposed method is a positioning method based on a simple deployment. In this method, the magnetism of the SMM is assumed to be detected using a smartphone application and by the 3D position of the smartphone. Just deploying a single SMM allows estimating the 3D position of the smartphone with a few centimeters in a range of 3 m area from the SMM. In the conventional method, installing transmitters is necessary for accuracy. On the other hand, with this method, it is not necessary to change the setting according to the place where the SMM is installed, and it is not necessary to change the setting according to the user of the smartphone. For example, when it is necessary to know the 3D position of a smartphone during an event held for a certain period of time, installation costs can be greatly decreased by using our method.

The structure of this paper is shown below. In Section 2, we will describe related work about indoor positioning methods. Next, we will describe the new SMM developed in Section 3, and the 3D positioning methods are discussed in Section 4. Evaluation experiments of the positioning method are discussed in Section 5. Finally, Section 6 describes the summary and future tasks.

2. Related Work

2.1 Positioning Method based on Radio Waves

One positioning method uses radio waves from Wi-Fi access points. The advantage of this method is that there is no need to newly install equipment in an environment where Wi-Fi access points are installed.

Zandbergen et al. [1], Cheng et al. [2], and Alam et al. [3] studied a positioning method using the radio field intensity fingerprint from from Wi-Fi access points. However, these methods require recreating fingerprints when the environment changes. Zhuang et al. studied a method to create a radio field strength fingerprint in buildings using crowdsourcing [4].

Other methods based on radio waves use BLE (Bluetooth Low Energy) beacons. The advantage of this method is that the installation cost is relatively inexpensive and the running cost is relatively low because it is low-power consumption.

Park et al. [5] and Rida et al. [6] studied a positioning method by installing BLE beacons in a room. Urano et al. studied a method to distribute BLE tags to visitors at an event venue and estimate a position with a BLE scanner installed in the venue [7]. Quuppa [*1] is one of a number of commercial products using BLE. This product can estimate the position of the BLE device from the incident angle of radio waves within an accuracy of 0.1 m to 1 m.

One of the other methods based on radio waves is to use UWB (Ultra Wide Band). In this method, since short pulse waves are used, estimation accuracy tends to be high compared with methods using Wi-Fi access points and BLE beacons.

Zhang et al. studied a method using receiving radio waves emitted by tags and four receivers installed around them [8]. Ubisense Real Time Location System [*2] is a commercial product that uses UWB. This product achieves real-time two-dimensional positioning within an error of a few meters.

As we have said, there are various positioning methods based on radio waves. These positioning methods have estimation accuracy of several meters or more; those with the best accuracy are on the order of tens of centimeters. In addition, these positioning methods decrease estimation accuracy when there are people or obstacles in the environment. Therefore, methods based on radio waves are not suitable for our purpose.

2.2 Positioning Method based on Ultrasound

Nakamura et al. studied a 3D positioning method for smartphones using three speakers [9]. Angelis et al. studied a method using movable beacons to avoid the influence by obstacles and by multi-path [10]. Medina et al. studied a 3D positioning method using four beacons [11].

These positioning methods can estimate the 3D position of a smartphone within several centimeters. However, as with the method based on radio waves, the estimation accuracy of these positioning methods decreases when there are people or obstacles in the environment. In addition, since the speed of sound depends on the temperature of the air, it is necessary to measure the temperature of the room before estimation. Therefore, methods based on ultrasound are not suitable for our purpose.

2.3 Positioning Method based on Visible Light

VLP (Visual Light Positioning) is a positioning method based on visible light. In this method, the 3D position of a camera is estimated from the position of the LED lamp on the camera.

Kumaki et al. studied the 3D positioning and orientaion estimation of smartphones using four LED lamps [12]. Zhang et al. studied a 3D smartphone positioning method using one rounded LED light [13].

As described above, VPL can estimate the 3D position of a smartphone within a few centimeters. However, we cannot use this method when the LED lamps are not present in the environment or are hidden. Since it is assumed that smartphones are stored in clothes or bags, this method is not suitable for our purpose.

2.4 Positioning Method based on Static Magnetism

In previous research, Murata et al. studied an indoor positioning method using residual magnetism in a building [14], [20]. In this method, the residual magnetism in a building is measured in advance to create a fingerprint database, which is then used to estimate the indoor position. As a result of the evaluation experiments, they estimated a position of a smartphone with a mean error of 13.7 m.

Schlageter et al. studied a 3D positioning method using two-dimensional arrangement magnets [15]. In this method, they estimated the position of a hall sensor from the magnetism generated by the magnets.

IndoorAtlas [*3] is a commercial product using statistic magnetism. This product uses geomagnetism for positioning; it is possible to achieve two-dimensional smartphone positioning with estimation accuracy of 1 m to 2 m. It also reduces the cost of creating a fingerprint with crowdsourcing using smartphones.

Although these positioning methods can be used on smartphones, they are not suitable for our purposes because of their estimation accuracy and difficulty in 3D positioning.

2.5 Positioning Method based on Dynamic Magnetism

Paperno et al. studied a positioning method based on dynamic magnetism generated by producing a current flow in a spinning coil [16]. Similarly, Hu et al. studied a positioning method based on dynamic magnetism generated by three orthogonal coils [17]. In these methods, a magnetic sensor detects the dynamic magnetism at three different frequencies of several kHz, and the signals are used to estimate the 3D position of the magnetic sensor.

Pirkl et al. studied a positioning method based on dynamic magnetism at a low-frequency [18]. This method uses transmitter coils to generate magnetism at a low-frequency, which makes it possible to estimate the 3D position of a receiver composed of coils with an accuracy of better than 1 m^2.

Pirkl et al. also studied a proximity detection method for a smartphone and smartwatch using dynamic magnetism at a low-frequency [19]. In this method, 40 cm × 30 cm rectangular coils with 20 windings are placed in a room and used to detect the proximity of a smartphone and smartwatch within a range of 30 cm to 50 cm.

POLHEMUS [*4] is a commercial product using dynamic magnetism. This system enables real-time 3D positioning such as motion capture in which the subject wears one or more sensors that sense the magnetism generated by a dedicated device.

As can be seen from these methods, to achieve 3D smartphone positioning, it is necessary to use dynamic magnetism at a low-frequency and to develop a low-cost method to generate dynamic magnetism.

2.6 Positioning Method using a Spinning Magnetic Marker

To take advantage of 3D positioning methods based on dynamic magnetism for smartphones, studied a positioning method using an SMM (Spinning Magnet Marker). The SMM is a device that spins a strong magnet at a constant speed and generates dy-

---

namic magnetism at a low-frequency of approximately 10 Hz at most. Dynamic magnetism generated by an SMM can be detected by a smartphone's magnetic sensor. The merit of this device is that it uses a magnet to generate magnetism; therefore, it can reduce the cost of generating the magnetism compared method that makes current flow in a coil.

Takeshima et al. studied a method for detecting passenger with a smartphone using SMM. In this research, two SMMs with respective magnet spinning speeds of 4 and 6 Hz were installed at a distance r of 60 cm. A passage direction detection rate of 83% was achieved under the condition of a distance r to the pedestrian of 75 cm and a walking speed of 1.2 m/s.

In addition, Takeshima et al. studied a two-dimensional positioning method using SMM [22]. As a result of the experiment with a magnet spinning speed of 6 Hz, they estimated the distance r within 13 cm and the azimuth angle θ with a mean error of 24° given a distance r of 2 m between the smartphone and the SMM.

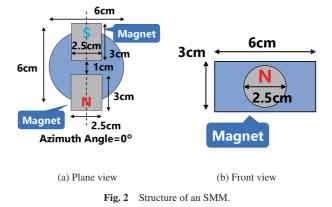## 3. Spinning Magnet Marker

3.1 Improvement Concepts

The following two points need to be considered when creating a smartphone 3D positioning method. The first method is to obtain the motor angle. Our previous study [22] determined the direction of the magnet with two Hall sensors installed around the magnet. Therefore, the azimuth angle θ can be estimated in 8 directions of 45° increments. To achieve 3D positioning within several centimeters, an azimuth angle θ is preferably obtained in increments of a few degrees. Therefore, it is necessary to obtain the motor angle by a mechanism different from the SMM used in previous research. The second point is the strength and shape of the magnet. Since the SMM is assumed to be installed indoors, it is necessary to determine the strength and shape of the magnet in consideration of safety so that the pedestrians and equipment are not affected.

3.2 Design of the SMM

A stepper motor will likely be used to acquire the motor angle. Since the stepper motor can obtain the motor angle every time time, it is possible to estimate the azimuth angle θ for each step angle. In addition, to estimate the azimuth angle θ using the stepper motor, we use a motor driver to control the motor and a device for recording the motor angle.

Takeshima et al. considered a magnet used for the SMM as follows. First, we should consider the influence of magnetism on a pacemaker. The pacemaker is designed to be unaffected by magnetism below 1 mT. Since the position of the pacemaker is assumed to be the height of the heart, it is around 1.4 m. Therefore, when setting the SMM at a height of 1 m, the influence on the height of the heart is considered to be small.

Second, we consider the influence of magnetism on a magnetic card. When the magnetic card is in a pants pocket, it is assumed to be at a height of about 1 m. Therefore, the magnetic card may be greatly affected by the magnetism generated by the SMM. Takeshima et al. adopt magnets that do not affect magnetic cards, i.e., magnets whose magnetic strength is less than 16 mT at
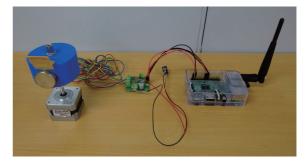

(a) Plane view   (b) Front view

Fig. 2   Structure of an SMM.

Fig. 3   The SMM in this research.

a distance of 10 cm from the SMM. Since this research situation is the same as that of Takeshima et al., we use the same magnets. The magnets have a cylindrical shape with a diameter of 25 mm and a length of 30 mm, and materials with a coercivity of 10,000 Oe to 10,500 Oe and a remanence of 14,300 G to 14,800 G are used.

Next, we consider how to install the magnet on a motor. Since it is difficult to mount the magnet directly on a rotating shaft of the motor, it is necessary to prepare a base for mounting the magnet. As mentioned above, since we use the same shape magnets as in our previous work, we also use the same base as in our previous work. **Figure 2** shows a plan view and a front view of the base. The base is a cylindrical type with a diameter of 6 cm and a height of 3 cm, and two magnets are mounted 1 cm apart from each other. At this time, we arrange the two magnets so that the N pole and the S pole face outward.

3.3 Implementation

We adopt MERCURY MOTOR SM-42BYG011-25 as a stepper motor of the SMM. Since a step angle of this motor is 3.6°, it is now able to estimate the azimuth angle θ in 100 directions. The base for attaching the magnet to the motor is made with a 3D printer and fixed to the rotating shaft of the motor. Next, we connect this stepper motor to a motor driver and a Raspberry Pi [*5]. This makes it possible to control the spinning of the motor and record a motor angle every time in the Raspberry Pi. **Figure 3** shows the SMM developed in this research.

4. Smartphone 3D Positioning Method

Here, we will show a smartphone 3D positioning method. First, we studied the magnetism generated by an SMM using a

---
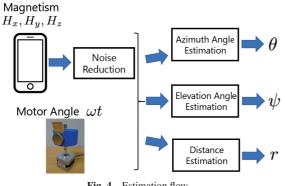
[*5]   https://www.raspberrypi.org

Fig. 4 Estimation flow.

simulator. Next, we formulate the magnetism generated by the SMM and consider the relationship between the orthogonal coordinate components of the magnetism and a 3D position from these formulas. Finally, we will show a noise reduction process for improving estimation accuracy and expanding coverage.

Figure 4 shows the flow of the 3D positioning method described in this section. First, the noise reduction process is applied to magnetic data measured by a smartphone in an experiment. Then, the azimuth angle θ, the elevation angle ψ, and the distance r are estimated from magnetic data after noise reduction and the motor angle of the SMM.

4.1 Simulation of Magnetism Generated by an SMM

We use a simulator named Qm [*6] to study the characteristics of magnetism generated by the SMM. It is possible to set physical properties such as the BH curve and the motion of the magnet and obtain magnetism at arbitrary positions. We set the simulator as follows. First, since it is not possible to specify the magnetic material in a cylinder with this simulator, the shape of the magnet is a rectangular parallelepiped with a width of 2.22 cm, a height of 2.22 cm, and a depth of 3 cm to obtain the same volume as that of the implemented cylindrical magnet, and the two magnets are placed 1 cm apart with the origin between them. The BH curve has a remanence of 14,300 G and coercivity of 10,000 Oe. Next, the magnet is spun counterclockwise around the z axis at a constant velocity of 5 °/s, and the time step was set at 1/72 second intervals.

Figure 5 shows the simulation results at the azimuth angle $\theta = 0°$, the distance $r = 1$ m, the elevation angle $\psi = 0°, 30°, 60°, 90°$. As shown in this figure, while the magnet spins once, the magnetism data draws a trajectory close to an ellipse. As the elevation angle ψ increases, the tilt of this ellipse changes; it becomes almost vertical at the elevation angle $\psi = 60°$. In addition, even given the same distance $r = 1$ m, the long axis of the ellipse decreases as the elevation angle ψ increases, and the shape becomes a circle at elevation angle $\psi = 90°$.

As shown in the simulation results, the magnetism generated by the SMM depends on the 3D position. When we know the relationship between the magnetism and the 3D position, we can estimate the 3D position of the smartphone from the magnetism. In the next section, to study the 3D positioning method, we will formulate the magnetism generated by the SMM.
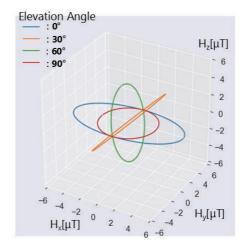
[*6]   http://www.slock.co.jp/Qm3/index.html

Fig. 5 Simulation results of the magnetism generated by an SMM.
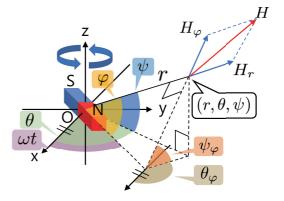

Fig. 6 Magnetic field generated by an SMM.

4.2 Formulation of Magnetism Generated by an SMM

We define a magnetic vector in a 3D polar coordinate system, as shown in **Fig. 6**, and use ω to denote the spinning speed of the motor and t to denote time. We assume that the magnetism generated by a magnet can be approximated as magnetism generated by a magnetic dipole. For simplicity, we consider only the case of an azimuth angle $\theta = 0°$. The magnetism equations can be written as follows:

$$H_x = H_r \cos \varphi \cos \psi + H_\varphi \sin \varphi \cos \psi_\varphi \cos \theta_\varphi \tag{1}$$

$$H_y = H_\varphi \sin \varphi \cos \psi_\varphi \sin \theta_\varphi \tag{2}$$

$$H_z = H_r \cos \varphi \sin \psi + H_\varphi \sin \varphi \sin \psi_\varphi \tag{3}$$

Next, from Fig. 6, we can derive the relationships between φ, θ_φ, ψ_φ and the azimuth angle θ, the elevation angle ψ, and the motor angle ωt:

$$\cos \varphi = \cos \psi \cos \omega t \tag{4}$$

$$\cos \theta_\varphi = \sin \omega t \frac{\cos^2 \psi \sin \omega t \cos \omega t}{\sqrt{1 - \cos^2 \psi \cos^2 \omega t (1 + \sin^2 \psi)}}$$
$$- \cos \omega t \sqrt{1 - \frac{\cos^4 \psi \sin^2 \omega t \cos^2 \omega t}{1 - \cos^2 \psi \cos^2 \omega t (1 + \sin^2 \psi)}} \tag{5}$$

$$\cos \psi_\varphi = \sqrt{\frac{1 - \cos^2 \psi \cos^2 \omega t (1 + \sin^2 \psi)}{1 - \cos^2 \psi \cos^2 \omega t}} \tag{6}$$

The relationships between the azimuth angle θ and the magnetism

and between the elevation angle ψ and the magnetism can be derived using these equations.

4.3 Azimuth Angle θ Estimation

The azimuth angle θ of a smartphone with respect to an SMM can be estimated from the magnetic norm and motor angle. The magnetic norm at the smartphone can be written as shown in Eq. (7) based on Eqs. (1)~(6).

$$H = \sqrt{H_\varphi^2 + (H_r^2 - H_\varphi^2)\cos^2\psi\cos^2\omega t} \tag{7}$$

This equation indicates that when $\omega t = \theta$, the magnetic norm is at its maximum. In other words, we can estimate the azimuth angle θ from the motor angle ωt at which the magnetic norm is maximal. However, as the motor spins through 1 period, there are two corresponding azimuth angles θ for which the norm is maximal. Thus, there is a problem of degeneracy, leading to two estimates of the azimuth angle θ.

4.4 Elevation Angle ψ Estimation

The elevation angle ψ of the smartphone with respect to the SMM can be from the magnetism components in orthogonal coordinates, H_x, H_y, and H_z. To this end, it is necessary to estimate the orientaion of the smartphone beforehand and transform the smartphone coordinate system to coincide with that of the SMM; however, we will not discuss this transformation procedure at this time. Equations (8) and (10) can be derived by substituting $\omega t = 0°$ into Eqs. (4), (5) and (6), and substituting the resulting equations into Eqs. (1) and (3). Equation (9) can be derived by substituting $\omega t = 90°$ into Eqs. (4), (5) and (6) and substituting the resulting equations into Eq. (2).

$$H_x = -H_\varphi + (H_r + H_\varphi)\cos^2\psi \tag{8}$$

$$H_y = H_\varphi \tag{9}$$

$$H_z = (H_r + H_\varphi)\cos\psi\sqrt{1 - \cos^2\psi} \tag{10}$$

Finally, the following equation can be derived by Eqs. (8), (9) and (10) for the elevation angle ψ:

$$\psi = \arccos\left(\frac{H_x + H_y}{\sqrt{(H_x + H_y)^2 + H_z^2}}\right) \tag{11}$$

H_x and H_z are maximal when the motor angle $\omega t = \theta$. H_y is maximal when the motor angle $\omega t = \theta + 90°$. We can estimate the elevation angle ψ by substituting the amplitude of each magnetism component H_x, H_y, H_z into Eq. (11).

However, unlike in the case of norm-based estimation of the azimuth angle θ, since the orthogonal components H_x, H_y and H_z of the magnetism depend on the orientaion of the smartphone, it is necessary to first estimate the orientaion of the smartphone.

4.5 Distance r Estimation

The distance r of the smartphone from the SMM can be estimated from the magnetic norm H, which depends on the distance r from the SMM. The magnetism generated by a magnet can be approximated as a magnetic dipole field. Therefore, we assume that the magnetism generated by the magnet along its central axis

is inversely proportional to the distance r. To study the difference in estimation accuracy obtained using different approximation curves, we derive two approximation curves with the forms shown in Eqs. (12) and (13). In these equations, A_1, B_1, C_1, A_2, and B_2 are fitting parameters.

$$H = A_1 r^{-B_1} + C_1 \tag{12}$$

$$H = A_2 r^{-B_2} \tag{13}$$

However, there is a problem in this method. As we mentioned in Section 4.1, the distance r dependence of the magnetic norm also depends on the elevation angle ψ. For example, when the elevation angle $\psi = 30°$, the magnetic norm decreases earlier than when the elevation angle $\psi = 0°$.

Therefore, the approximate curve cannot be used for distance r estimation at an arbitrary elevation angle ψ. If we examine the distance dependence of the magnetic norm for all elevation angles ψ, this problem may be solvable. However, this approach is not practical because the number of data that must be studied is enormous. Therefore, it is necessary to consider a new method that can be estimated even at the arbitrary elevation angle ψ.

To derive an equation that estimates the distance r with an arbitrary elevation angle ψ, we further consider Eq. (7) derived in Section 4.3. This time, we approximate a cylindrical magnet as a magnetic dipole. It is known that the radial direction of magnetism generated by a magnetic dipole and the component perpendicular thereto are inversely proportional to the cube of the distance r. Therefore, H_r, H_φ in Eq. (7) can be expressed as follows.

$$H_r = \frac{H_r'}{r^3} \tag{14}$$

$$H_\varphi = \frac{H_\varphi'}{r^3} \tag{15}$$

From these relationships, Eq. (7) can be written as below.

$$H = \sqrt{\left(\frac{H_\varphi'}{r^3}\right)^2 + \left(\left(\frac{H_r'}{r^3}\right)^2 - \left(\frac{H_\varphi'}{r^3}\right)^2\right)\cos^2\psi\cos^2\omega t} \tag{16}$$

The following equation is derived from this Eq. (16).

$$r = \frac{\left(H_\varphi^{2\prime} + (H_r^{2\prime} - H_\varphi^{2\prime})\cos^2\psi\cos^2\omega t\right)^{\frac{1}{6}}}{H^{\frac{1}{3}}} \tag{17}$$

When you know the constant H_r', H_φ' in this equation, the distance r can be estimated from the measured magnetic norm H and the estimated elevation angle ψ. Therefore, next, we derive the constant H_r', H_φ'. Here, when the elevation angle $\psi = 0°$, we obtain the Eq. (15) as follows.

$$r = \frac{\left((H_\varphi^{2\prime} + (H_r^{2\prime} - H_\varphi^{2\prime})\cos^2\omega t\right)^{\frac{1}{6}}}{H^{\frac{1}{3}}} \tag{18}$$

Furthermore, when the motor angle is $\omega t = 0°$, the above equation becomes the following equation.

$$H_r' = r^3 H \tag{19}$$

In other words, when we measure the value of the magnetic norm H at the elevation angle $\psi = 0°$, the distance $r = 1$ m at the motor angle $\omega t = 0°$, and one can then find the constant H_r' from

Eq. (17). The constant H'_φ can be derived in the same way. When the elevation angle $\psi = 0°$ and when the motor angle $\omega t = 90°$, Eq. (15) is as follows.

$$H'_\varphi = r^3 H \tag{20}$$

We substitute the constant H'_r, H'_φ derived by these methods into Eq. (17) to estimate the distance r.

4.6 Noise Reduction Process

Here, we will present a procedure for reducing the influence of noise in the measured magnetic data. As the distance r from the SMM increases, the influence of noise becomes stronger than the influence of the magnetism generated by the SMM, and it becomes difficult to identify the magnetism generated by the SMM in the magnetic data. We describe the process applied to the magnetic data, and as an example of this process, we present a case of x-component magnetic data measured at the azimuth angle $\theta = 0°$, the elevation angle $\psi = 0°$ and the distance $r = 2$ m from the SMM.

4.6.1 Averaging

When we assume that the noise contained in the magnetic data is random, we expect that the influence of the noise can be reduced by averaging the magnetic data. First, we select a data segment corresponding to a measurement time of 10 seconds from the measured magnetic data, and we divide these data into 10 1-second intervals, corresponding to the rotation period of the motor. Then, the times associated with these ten data intervals are reset to 0 to 1 seconds, and the data are averaged. **Figure 9** (a) shows a comparison between the magnetism before the averaging process and after.
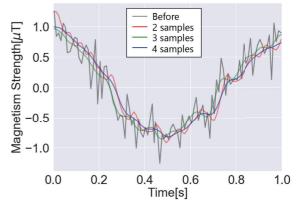
4.6.2 Smoothing

Although the influence of noise is reduced by the process described above, some of this influence remains. Therefore, we also apply a procedure to calculate the moving average to the magnetic data as an additional process step. To achieve appropriate smoothing, we calculated several moving averages with different window widths and different numbers of iterations and compared the results.
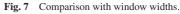
Figure 7 shows the results obtained using several window widths with the number of iterations fixed at 5 times. Although the smoothing is insufficient with a window width of 2 samples, effective smoothing is achieved with a window width of 3 sam-

ples, and the results show no noticeable change with a window width greater than 3 samples. From these observations, we can determine that a window width of 3 samples is sufficient for the smoothing process.

Figure 8 shows the results obtained by fixing the window width to 3 samples and varying the number of iterations of the moving average procedure. The smoothing does not appear to be sufficient when the number of iterations is 5; however, no further noticeable change occurs after 10 iterations. From these findings, we can determine that 10 iterations of the moving average procedure is sufficient.

Based on the above results, we smooth the magnetic data using a window width of 3 samples and 10 iterations of the moving average procedure. Figure 9 (b) shows a comparison between the

Fig. 7 Comparison with window widths.

Fig. 8 Comparison with number of iterations.

(a) Before averaging and after

(b) Before smoothing and after

(c) The magnetism and the approximation curve

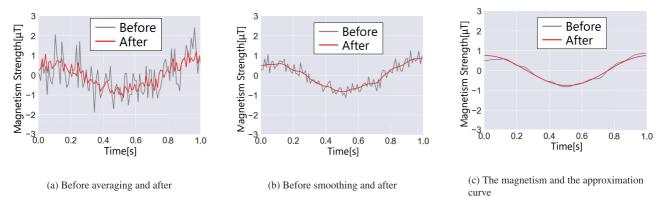**Fig. 9** Noise reduction process at the azimuth angle $\theta = 0°$, the elevation angle $\psi = 0°$, and the distance $r = 2$ m.

magnetism before the smoothing process and after.

4.6.3 Curve Fitting

Approximation curves for each component of the magnetic data can be derived through curve fitting of the data obtained after the previously described process. As discussed in Section 4.6, we perform sinusoidal curve fitting using the functional form defined in Eq. (21) on the magnetism strength data measured by the magnetic sensor. In addition, we assume that the spinning speed of the SMM is already known to be 1 Hz. In the equation below, h denotes the magnetism and D, E and F are fitting parameters.

$$h = D \sin(2\pi(\omega t + E)) + F \tag{21}$$

The procedure described above is applied to the magnetic data for each component corresponding to the x, y, and z axes, and the azimuth angle θ, the elevation angle ψ, and the distance r are then estimated from these three approximation curves. Figure 9 (c) shows a comparison between the magnetism and the approximation curve.

5. Evaluation Experiment

Here, we will describe the evaluation experiment of the 3D positioning method considered in Section 4. First, we will describe the setting of the SMM in the evaluation experiment, including the estimated positions and the measuring time. Next, we will describe preliminary experiments that estimate the azimuth angle θ, the elevation angle ψ, and the distance r separately. Finally, we will describe experiments to evaluate the estimation accuracies of the azimuth angle θ, the elevation angle ψ, and the distance r simultaneously at each 3D position of a smartphone.

5.1 Experimental System

Figure 10 shows the experimental system. The system is composed of a smartphone, an SMM, and a PC. Before the experiment, we synchronized the time of the smartphone and Raspberry Pi with NTP (Network Time Protocol). Next, we activate an application for measuring magnetism on the smartphone. At the start of the experiment, a signal is sent from the PC to the SMM to spin magnets, and when the measurement time is over, the spinning of the magnet is stopped. At this time, motor angle ωt data are recorded in the Raspberry Pi, and the magnetism data
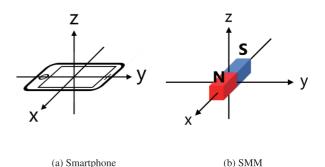
are recorded on the smartphone. After the experiment, we transmit the motor angle ωt data recorded in the Raspberry Pi and the magnetism data recorded on the smartphone to the PC; we substitute the data into equations derived in Section 4.2 to calculate the 3D position of the smartphone.

We will describe the setting of the experiment as follows. The spinning speed of the motor of the SMM was 1 Hz. The smartphone is the iPhone 6 Plus, and the sampling frequency of the magnetic sensor is 100 Hz, which is the settable upper limit value. **Figure 11** shows the coordinate system of the smartphone and the SMM in the experiment. As shown in Fig. 11 (b), the direction from the south pole to the north pole of the magnet at the motor angle $\omega t = 0°$ is set as the positive direction of the x-axis of the right-handed orthogonal coordinate system. In addition, as shown in Fig. 11 (a), the coordinate system of the smartphone is set, and the orientaion is fixed to coincide with the coordinate system of the SMM, and the experiments are conducted. The measurement time is set to 15 seconds per one experiment for the noise reduction process described in Section 4.6. In addition, to calculate the average and the standard deviation of the estimation results, measurements are made ten times at each estimated position.

When estimating the elevation angle ψ, it is difficult to measure by changing the elevation angle ψ while maintaining a constant distance r. It is necessary to put the smartphone on the base and measure it. Therefore, we estimate the elevation angle ψ by turning the SMM and the smartphone sideways in the same direction. **Figure 12** shows the state at the time of the experiment. Figure 12 (b) is when the elevation angle $\psi = 0°$. To reduce the influence of the magnetism from the surroundings, the SMM and the smartphone are installed on a plastic base about 1 m in height. While keeping these bases parallel, we change the distance r and measure the azimuth angle θ. Figure 12 (a) is when the elevation angle $\psi = 30°$. As described above, we turn the SMM and

(a) Smartphone   (b) SMM

Fig. 11 Coordinate system.

Fig. 10 System configration.

(a) Experiment for elevation angle ψ estimation   (b) Experiment for azimuth angle θ estimation

Fig. 12 Experimental setup.

Table 2 Result of estimated azimuth angle θ.

Azimuth angle[°]	0		45		90		135		180	
	θ_1	θ_2	θ_1	θ_2	θ_1	θ_2	θ_1	θ_2	θ_1	θ_2
Mean Error[°]	10	9	11	10	1	4	6	3	4	2
Standard Deviation[°]	5	3	3	3	5	5	6	3	6	6

Table 3 Result of estimated elevation angle ψ.

Elevation angle[°]	−60		−30		0		30		60	
	ψ_1	ψ_2	ψ_1	ψ_2	ψ_1	ψ_2	ψ_1	ψ_2	ψ_1	ψ_2
Mean Error[°]	8	10	5	2	4	3	3	4	0	4
Standard Deviation[°]	10	2	2	2	1	1	1	1	2	2

Fig. 13 Estimation accuracy of azimuth angle θ in Section 5.2.1.

Fig. 14 Magnetic data at each elevation angle ψ.

the smartphone sideways, keep the elevation angle ψ constant, change the distance r and measure the elevation angle ψ. The results of preliminary experiments are shown in the next section.

5.2 Prior Experiment

We estimate the azimuth angle θ, the elevation angle ψ, and the distance r separately as a preliminary experiment. In this section, we describe each experiment and evaluate its estimation accuracy.

5.2.1 Evaluation of Azimuth Angle θ Estimation

We fix the distance r between the smartphone and the SMM to 1 m and performed measurements at 8 azimuthal positions of $\theta = 0°, 45°, 90°, 135°, 180°, 225°, 270°$ and $315°$. The measurement time is 15 seconds, and estimation is performed 10 times at each position. **Table 2** shows the results. The estimation results presented in this table are rounded off to the nearest whole number. As mentioned in Section 4.3, the proposed method estimates two azimuth angles θ. We denote these two azimuth angles by θ_1 and θ_2. The mean error is obtained by taking the absolute value of the difference between the true azimuth angle θ value and the average of the 10 azimuth estimates.
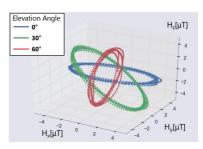
Next, to study the relationship between the estimation accuracy and the distance r from the SMM, we fix the true azimuth angle θ and the elevation angle $\psi = 0°$ and estimate the azimuth angle θ at 8 positions ranging from 50 cm to 4 m from the SMM in intervals of 50 cm. The measurement time is 15 seconds, and estimation is performed 10 times at each position. **Figure 13** shows the results. The estimation results presented in this figure are rounded off to the nearest whole number. The estimation results at distances of up to 3 m have a maximum mean error within 14° and standard deviation within 12°. By contrast, for the measurements at 3.5 m and 4 m, although the mean error is within 11°, the standard deviation is more than 30°, indicating that the stability of the estimation is decreasing.

5.2.2 Evaluation of Elevation Angle ψ Estimation

We fixed the distance r from the smartphone to the SMM to 1 m and perform measurements at 5 positions separated by intervals of 30°. The measurement time is 15 seconds, and the estimation is performed 10 times at each position. Since two azimuth angles are estimated, two elevations are also estimated. We denote the

two estimated elevation angles by ψ_1 and ψ_2. In addition, we experiment with transforming the smartphone coordinate system to coincide with the SMM coordinate system.

Table 3 shows the estimation results rounded off to the nearest whole number. The mean error of the elevation estimates is within 10°; thus, the estimation accuracy for the elevation ψ can be considered nearly identical to that for the azimuth angle θ. The standard deviation of the elevation angle ψ estimation is within 2° except for the elevation angle $\psi = -60°$. This standard deviation is lower than that of the azimuth angle θ estimation. This difference is attributed to the smaller effect of the rotation stability of the motor at the elevation angle ψ estimation compared with the estimation of the azimuth angle θ, which depends on the motor angle ωt. In addition, the increase in the standard deviation only at an elevation angle of −60° is considered to be an effect of turning the SMM sideways.

Figure 14 shows the magnetic data measured while estimating the elevation angles ψ. From this figure, we can see that the magnetism vectors generated by the SMM form a shape close to an ellipse around the smartphone. As the elevation angle ψ increases, this ellipse becomes tilted, and it is nearly vertical at an elevation of $\psi = 60°$. This tendency agrees with the simulation result of Fig. 5 discussed in Section 4.1.

5.2.3 Evaluation of Distance r Estimation

To estimate the distance r of the smartphone from the SMM, we first need to study the relationship between the amplitude of the magnetic norm and the distance from the SMM. To do this, we measure the magnetism at various distances from the SMM in increments of 10 cm. We fix the azimuth angle $\theta = 0°$ and the elevation angle $\psi = 0°$, and the measurement time is 15 seconds. We apply the process described in Section 4.6 to the magnetic data obtained in this experiment to obtain approximation curves describing the behavior of the magnetic norm over time. We subtract the minimum value from the maximum value of each approximation curve and divided the result by 2 to obtain the norm amplitude. We derive the approximation curves by applying curve fitting to 38 data segments using Eqs. (12) and (13) presented in Section 4.5. We refer to Eq. (12) as approximation curve 1 and to Eq. (13) as approximation curve 2. The curve fitting
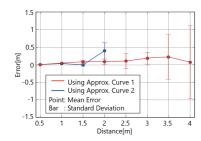
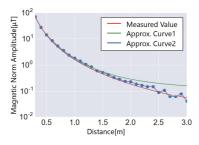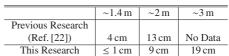**Fig. 15** Estimation accuracy of distance r in Section 5.2.3.

Fig. 16 Norm amplitude (0.3 m~3 m).

Table 4 Mean error of estimated distance r compared with previous research.

	~1.4 m	~2 m	~3 m
Previous Research (Ref. [22])	4 cm	13 cm	No Data
This Research	≤ 1 cm	9 cm	19 cm

Fig. 17 x-axis power spectrum at 3 m.

Fig. 18 x-axis power spectrum at 3.5 m.

yielded parameters of $A_1 = 1.590$, $B_1 = 3.146$ and $C_1 = 0.111$ for approximation curve 1 and parameters of $A_2 = 1.636$ and $B_2 = 3.124$ for approximation curve 2. These two approximation curves can both be considered to provide reasonable approximations of the magnetism, as indicated by the decision coefficients of 0.9997 for curve fit 1 and 0.9996 for curve fit 2. **Figure 16** presents the curve fitting results.

We then estimate the distance r from the smartphone to the SMM using the derived approximation curves. We estimate the distance r at 8 positions at distances ranging from 50 cm to 4 m in increments of 50 cm. The measurement time is 15 seconds, and estimation is performed 10 times at each position. **Figure 15** shows the estimation results which are rounded off to the nearest third decimal place. The results obtained using approximation curve 1 are higher in accuracy than those obtained using approximation curve 2 for distances of up to 1.5 m. However, distances greater than 2.5 m could not be successfully estimated using approximation curve 1. The reason for this, as shown in Fig. 16, is that approximation curve 1 begins to deviate from the measured data at distances greater than 1 m. In addition, when the norm amplitude is smaller than $C_1 = 0.111$, then distance r estimation using this curve becomes impossible because there is no corresponding distance value. By contrast, the estimation accuracy of the estimation results obtained using approximation curve 2 is higher than that for approximation curve 1 at distances greater than 2 m, and it is possible to estimate distances of more than 2.5 m using approximation curve 2. Up to a distance r of 3 m, the mean error is no more than 19 cm, and the standard deviation is 17 cm. At distances r of 3 m and 3.5 m, the mean errors are no more than 22 cm, however the standard deviations are respectively more than 50 cm and 1 m at these distances. These findings indicate that the stability of the estimation decreases as the distance increases. **Table 4** presents a comparison with our previous research [22]. The results indicate improvement compared with our previous study.
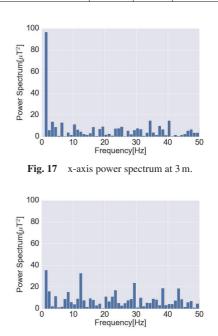
5.2.4 Coverage of an SMM

We study a coverage of magnetism generated by an SMM. **Figures 17**, **18** show a power spectrum of the x-axis component of magnetism at respective distances of 3 m and 3.5 m. In the power spectrum at a distance $r = 3$ m, a power spectrum peak appears at 1 Hz, which is the spinning speed of the motor. However, at the distance $r = 3.5$ m, the power spectrum peak at 1 Hz is approximately the same strength as the noise, and it becomes difficult for a smartphone to detect the magnetism generated by an SMM. The standard deviation in the estimation results increases along with a greater distance increases. Therefore, the influence of noise can no longer be sufficiently reduced by the method presented in Section 4.6.1.

5.3 Smartphone 3D Positioning

Up to this point, we have separately estimated the azimuth angle θ, the elevation angle ψ, and the distance r. In this section, we conduct experiments simultaneously to evaluate accuracies of the azimuth angle θ, the elevation angle ψ, and the distance r at each 3D position.

5.3.1 Measurement Positions

According to the experimental result in Section 5.2.1, the estimation accuracy of the azimuth angle θ is approximately equivalent when the elevation angle ψ and the distance r are fixed. Therefore, the azimuth angle θ is fixed to $\theta = 0°$. The elevation angle ψ is measured from $-60°$ to $60°$ in increments of $30°$ as in Section 5.2.3. As discussed in Section 5.2.4, it is difficult for a smartphone's magnetic sensor to detect magnetism by an SMM at a distance of $r = 3.5$ m or more. Therefore, a minimum distance r to be measured $r = 50$ cm, a maximum distance $r =$
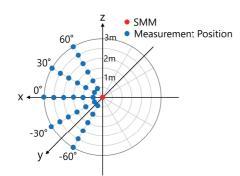
Fig. 19 Measurement positions.

(a) $\theta = 0°, \psi = 0°, r = 0.5$ m, 1 m, 1.5 m, 2 m, 2.5 m, 3 m

(b) $\theta = 0°, \psi = 30°, r = 0.5$ m, 1 m, 1.5 m, 2 m, 2.5 m, 3 m

(c) $\theta = 0°, \psi = -30°, r = 0.5$ m, 1 m, 1.5 m, 2 m, 2.5 m, 3 m

(d) $\theta = 0°, \psi = 60°, r = 0.5$ m, 1 m, 1.5 m, 2 m, 2.5 m, 3 m

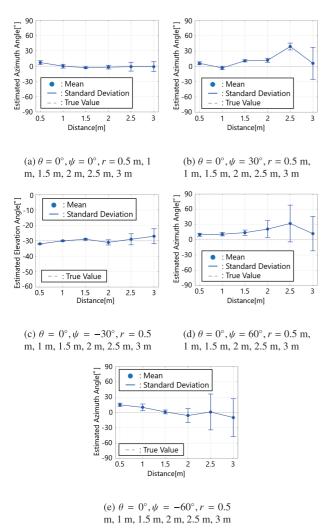(e) $\theta = 0°, \psi = -60°, r = 0.5$ m, 1 m, 1.5 m, 2 m, 2.5 m, 3 m

Fig. 20 Estimation accuracy of azimuth angle θ in Section 5.4.

3 m, and the distance r was estimated at intervals of 50 cm. We set a measurement distance r from 0.5 m to 3 m.

In other words, the measured positions are the azimuth angle $\theta = 0°$, the elevation $\psi = -60°, -30°, 0°, 30°, 60°$, and the distance $r = 50$ cm, 1 m, 1.5 m, 2 m, 2.5 m, 3 m for each elevation angle ψ, a total of 30 places. **Figure 19** shows the measurement positions. In this experiment, for each measurement position, the measurement time is 15 seconds, the number of measurements is 10 times, and the mean and standard deviation of the estimation accuracy are derived from the result.
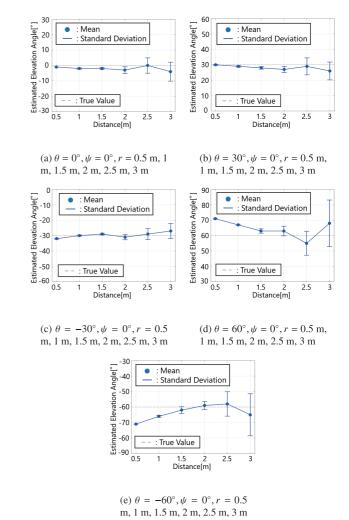

(a) $\theta = 0°, \psi = 0°, r = 0.5$ m, 1 m, 1.5 m, 2 m, 2.5 m, 3 m

(b) $\theta = 30°, \psi = 0°, r = 0.5$ m, 1 m, 1.5 m, 2 m, 2.5 m, 3 m

(c) $\theta = -30°, \psi = 0°, r = 0.5$ m, 1 m, 1.5 m, 2 m, 2.5 m, 3 m

(d) $\theta = 60°, \psi = 0°, r = 0.5$ m, 1 m, 1.5 m, 2 m, 2.5 m, 3 m

(e) $\theta = -60°, \psi = 0°, r = 0.5$ m, 1 m, 1.5 m, 2 m, 2.5 m, 3 m

Fig. 21 Estimation accuracy of elevation angle ψ in Section 5.4.

5.4 Result of 3D Positioning

The 3D positioning result consists of estimation results of the azimuth angle θ, the elevation angle ψ and the distance r for each measurement position. To examine the distance dependence of each estimation result, these estimation results are plotted for each azimuth angle θ, elevation angle ψ, and distance r.

We will evaluate the estimation accuracy of the azimuth angle θ. **Figure 20** shows the estimation result of the azimuth angle θ at each measurement position. These estimation results are rounded off to the nearest decimal point, and the standard deviation is rounded to the first decimal place. Although the azimuth angle θ takes a value from $0°$ to $360°$, for calculating the mean azimuth angle θ, the azimuth angle θ takes a value from $-180°$ to $180°$. In addition, as described in Section 4.3, although there are two estimated azimuth angles θ in this method, these estimation results are almost the same; therefore, we omit the results in this time.

For all results up to distance $r = 1$ m, the mean is within $\pm 15°$, and the standard deviation is within $6°$. On the other hand, for results greater than a distance of $r = 2.5$ m, the mean and the standard deviation increase. Even with the estimation at the same distance r, the standard deviation increases as the elevation angle ψ increases. The standard deviation increases as the distance r increases because the effect of magnet is thought to decrease.
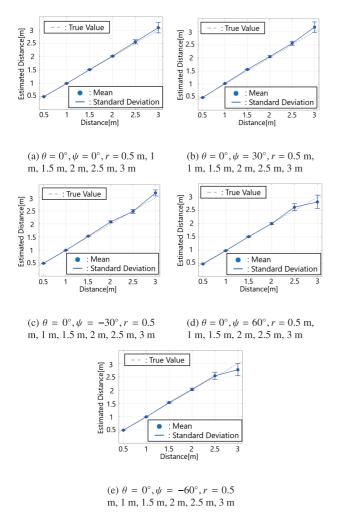
(a) $\theta = 0°, \psi = 0°, r = 0.5$ m, 1 m, 1.5 m, 2 m, 2.5 m, 3 m

(b) $\theta = 0°, \psi = 30°, r = 0.5$ m, 1 m, 1.5 m, 2 m, 2.5 m, 3 m

(c) $\theta = 0°, \psi = -30°, r = 0.5$ m, 1 m, 1.5 m, 2 m, 2.5 m, 3 m

(d) $\theta = 0°, \psi = 60°, r = 0.5$ m, 1 m, 1.5 m, 2 m, 2.5 m, 3 m

(e) $\theta = 0°, \psi = -60°, r = 0.5$ m, 1 m, 1.5 m, 2 m, 2.5 m, 3 m

Fig. 22   Estimation accuracy of distance r in Section 5.4.

Therefore, the influence of noise cannot be sufficiently reduced by the method shown in Section 4.6.

When the absolute value of the elevation angle ψ is large, the standard deviation increases. As mentioned in Section 4.1, as the absolute value of the elevation angle ψ increases, the magnetic norm decreases. Therefore, estimating the azimuth angle θ is thought difficult compared to when the elevation angle $\psi = 0°$.

We will evaluate the estimation accuracy of the elevation angle ψ. **Figure 21** shows the estimation results of the elevation angle ψ at each measurement position. These estimation results are rounded off to the nearest hundred percent, and the standard deviations rounded to the first decimal place.

At the elevation angle $\psi = 0°$, when the distance r is within 2 m, the mean is within $3°$, and the standard deviation is within $2.2°$. On the other hand, when the distance r is greater than 2.5 m, the mean and the standard deviation tend to be large compared with other distances. This tendency is similar to estimation results with the elevation angle $\psi = 0°$. At the elevation angle $\psi = 60°$, when the distance $r = 1.5$ m or 2 m, the estimation accuracy is the best. On the other hand, when the distance $r = 0.5$ m or 1 m, the estimation accuracy is low; we approximated the magnetism generated by an SMM as the magnetism generated by the magnetic dipole in Section 4.2, and it is possible that this approximation is not valid at a distance r close to the magnet.

We will evaluate the estimation accuracy of the distance r. As described in Section 4.5, to estimate the distance r of a smartphone from an SMM at an arbitrary elevation angle ψ, we need to find the constant H'_r, H'_φ in Eq. (15). Therefore, we measured the magnetism for 15 seconds at a position of distance $r = 1$ m with azimuth angle $\theta = 0°$ and elevation angle $\psi = 0°$. Next, we applied the noise reduction process to the measured magnetism and checked the norm value at motor angles $\omega t = 0°$, $\omega t = 90°$. As a result, we found that $H'_r = 6.77\,\mu T$, $H'_\varphi = 3.04\,\mu T$. By substituting these constants into the Eq. (16), the estimated elevation angle ψ and the measured magnetism, we the estimate distance r from an SMM.

Figure 22 shows the estimation accuracy of the distance r at each measurement position. These estimation results are rounded off to their second decimal places on the average and rounded off to their fourth decimal places of the standard deviation.

When the elevation angle $\psi = 0°$, the mean is 2.01 m at distance $r = 2$ m, and the standard deviation is 7.8 cm. On the other hand, when the distance r is more than 2.5 m, both the mean and the standard deviation are large compared with other distances. Even when the elevation angle $\psi = \pm30°$, both the mean and the standard deviation are large when the distance is more than $r = 2.5$ m. As a whole, the estimation accuracy is lower than when the elevation angle $\psi = 0°$. When the elevation angle $\psi = \pm60°$, the tendency is more intense, and the estimation accuracy is lower than when the elevation $\psi = 30°$.

5.5   Limitation of Our Proposed Method

In this research, we assumed that the smartphone is stationary. However, there are not many situations where a person with a smartphone remains in the same position for more than 15 seconds. For noise reduction processing, we measure the spinning speed of the magnet at 1 Hz for 15 seconds, but the pedestrian moves several meters during the measurement. When the spinning speed of the magnet is set to 10 Hz, the measurement time is expected to be 1 second, but the pedestrian moves 1 m or more.

Increasing the spinning speed of the magnet can suppress the influence of the movement of the smartphone. However, as mentioned in Section 2.5, since the sampling frequency of the current smartphone is about 100 Hz, there is a limit to increasing the spinning speed of the magnet. Therefore, to put this method to practical use, it is necessary to propose a method to estimate a trajectory of the moving smartphone from the magnetism measured by the moving smartphone. For this purpose, it is necessary to extend the magnetism equations derived in Section 4.2 to the equations in which the position of the smartphone is time dependent. In addition, when a smartphone moves, the noise reduction process applied to improve the estimation accuracy proposed in Section 4.6 cannot be used. Therefore, we need to consider another method to improve estimation accuracy.

6.   Conclusion

In this study, we proposed a smartphone 3D positioning method using a Spinning Magnet Marker (SMM). The purpose of the proposed method is to estimate the 3D position of a smartphone to within several centimeters, to estimate the activities of

indoor people from the obtained data, and to use this information to market and develop new services.

In this study, to estimate the 3D position of a smartphone, we developed a new SMM that spins a powerful neodymium magnet to generate magnetoquasistatic field. We then derived equations between magnetism generated by the SMM and the 3D position. As a result of the evaluation experiments, at the azimuth angle $\theta = 0°$, the elevation angle $\psi = 0°$, and the distance r up to 3 m, the azimuth angle θ is estimated with a mean error of $1°$, the elevation angle ψ is estimated with a mean error of $4°$, and the distance r is estimated with a mean error of 9 cm.

In the proposed method, there is no limit on the number of smartphones that can estimate the 3D position with one SMM; the smartphone measures the magnetism generated by the SMM and estimates the 3D position of the smartphone from the magnetism and the spinning angle of the magnet of the SMM. Since the calculations to estimate the 3D position of the smartphone are performed by the smartphone itself, this method can estimate the 3D position of multiple smartphones with a single SMM.

As a future task, we plan to consider a method to estimate the orientaion of a smartphone. As mentioned in Section 4.4, the proposed method uses the orthogonal coordinate components of magnetism. Since the orthogonal components of magnetism depend on the orientaion of the smartphone, it is necessary to estimate the orientaion of the smartphone prior to the 3D positioning. When you estimate the direction of gravity using the acceleration sensor mounted on the smartphone, you may be able to estimate the orientaion of the smartphone from the magnetism generated by the SMM. When you estimate the orientaion of the smartphone, the proposed method in this research will be applicable even in cases where the smartphone is in a pocket or held in a hand.

Furthermore, we will consider a smartphone positioning method using multiple SMMs. In this study, the coverage of one SMM was an area with a radius of 3 m from the SMM. This coverage range can likely be expanded by using multiple SMMs.

References

[1] Zandbergen, P.A.: Accuracy of iphone Locations: A Comparison of Assisted GPS, WiFi and Cellular Positioning, *Trans. GIS*, Vol.13, No.s1, pp.5–25 (2009).

[2] Cheng, J., Cai, Y., Zhang, Q., Cheng, J. and Yan, C.: A New Three-Dimensional Indoor Positioning Mechanism based on Wireless Lan, *Mathematical Problems in Engineering*, Vol.2014, pp.1–7 (2014).

[3] Alam, S., Atif, S., Hussain, S. and Hussain, E.: 3-dimensional Indoor Positioning System based on Wi-Fi Received Signal Strength using Greedy Algorithm and Parallel Resilient Propagation, *International Journal of Computer Applications*, Vol.116, No.18, pp.32–38 (2015).

[4] Zhuang, Y., Syed, Z., Georgy, J. and El-Sheimy, N.: Autonomous Smartphone-Based wifi Positioning System by using Access Points Localization and Crowdsourcing, *Pervasive and Mobile Computing*, Vol.18, pp.118–136 (2015).

[5] Faragher, R. and Harle, R.: An Analysis of the Accuracy of Bluetooth Low Energy for Indoor Positioning Applications, *Proc. 27th International Technical Meeting of the Satellite Division of the Institute of Navigation* (*ION GNSS+'14*), pp.201–210 (2014).

[6] Rida, M.E., Liu, F., Jadi, Y., Algawhari, A.A.A. and Askourih, A.: Indoor Location Position based on Bluetooth Signal Strength, *Proc. 2015 2nd International Conference on Information Science and Control Engineering* (*ICISCE*), pp.769–773 (2015).

[7] Urano, K., Kaji, K., Hiroi, K. and Kawaguchi, N.: A Location Estimation Method using Mobile BLE Tags with Tandem Scanners, *Proc. 2017 ACM International Joint Conference on Pervasive and Ubiquitous Computing and Proc. 2017 ACM International Symposium on Wearable Computers*, pp.577–586 (2017).

[8] Zhang, C., Kuhn, M., Merkl, B., Mahfouz, M. and Fathy, A.E.: Development of an UWB Indoor 3D Positioning Radar with Millimeter Accuracy, *Proc. Microwave Symposium Digest, IEEE MTT-S International*, pp.106–109 (2006).

[9] Nakamura, M., Akiyama, T., Sugimoto, M. and Hashizume, H.: Rapid and Precise Indoor 3D Localization using Acoustic Signal for Smartphone, *Journal of Information Processing*, Vol.57, No.11, pp.2489–2500 (2016). (in Japanese).

[10] Medina, C., Segura, J.C. and De la Torre, A.: Ultrasound Indoor Positioning System based on a Low-Power Wireless Sensor Network Providing Sub-Centimeter Accuracy, *Sensors*, Vol.13, No.3, pp.3501–3526 (2013).

[11] De Angelis, A., Moschitta, A., Carbone, P., Calderini, M., Neri, S., Borgna, R. and Peppucci, M.: Design and Characterization of a Portable Ultrasonic Indoor 3-D Positioning System, *IEEE Trans. Instrumentation and Measurement*, Vol.64, No.10, pp.2616–2625 (2015).

[12] Kumaki, H., Akiyama, T., Hashizume, H. and Sugimoto, M.: 3D Indoor Positioning and Rapid Data Transfer using Modulated Illumination, *Proc. International Conference on Indoor Positioning and Indoor Navigation* (*IPIN*), Alcalá de Henares, pp.4–7 (2016).

[13] Zhang, R., Zhong, W.-D., Kemao, Q. and Zhang, S.: A Single Led Positioning System based on Circle Projection, *IEEE Photonics Journal*, Vol.9, No.4, pp.1–9 (2017).

[14] Murata, Y., Kaji, K., Hiroi, K., Kawaguchi, N., Kamiyama, T., Ohta, K. and Inamura, H.: Pedestrian Indoor Positioning Method using Magnetic Data, *Journal of Information Processing*, Vol.58, No.1, pp.57–67 (2017). (in Japanese).

[15] Schlageter, V., Besse, P.-A., Popovic, R.S. and Kucera, P.: Tracking System with Five Degrees of Freedom using a 2D-Array of Hall Sensors and a Permanent Magnet, *Sensors and Actuators A: Physical*, Vol.92, No.1, pp.37–42 (2001).

[16] Eugene Paperno, Ichiro Sasada, and Eduard Leonovich.: A New Method for Magnetic Position and Orientation Tracking, *IEEE Trans. Magnetics*, Vol.37, No.4, pp.1938–1940 (2001).

[17] Hu, C., Song, S., Wang, X., Meng, M.Q.H. and Li, B.: A Novel Positioning and Orientation System based on Three-Axis Magnetic Coils, *IEEE Trans. Magnetics*, Vol.48, No.7, pp.2211–2219 (2012).

[18] Pirkl, G. and Lukowicz, P.: Robust, Low Cost Indoor Positioning using Magnetic Resonant Coupling, *Proc. 2012 ACM Conference on Ubiquitous Computing*, pp.431–440 (2012).

[19] Pirkl, G., Hevesi, P., Cheng, J. and Lukowicz, P.: mbeacon: Accurate, Robust Proximity Detection with Smart Phones and Smart Watches using Low Frequency Modulated Magnetic Fields, *Proc. 10th EAI International Conference on Body Area Networks*, pp.186–191 (2015).

[20] Takeshima, C., Kaji, K., Hiroi, K., Kawaguchi, N., Kamiyama, T., Ohta, K. and Inamura, H.: A Pedestrian Passage Detection Method by using Spinning Magnets on Corridors, *Adjunct Proc. 2015 ACM International Joint Conference on Pervasive and Ubiquitous Computing and Proc. 2015 ACM International Symposium on Wearable Computers*, pp.411–414 (2015).

[21] Takeshima, C., Kaji, K., Hiroi, K. Kawaguchi, N., Kamiyama, T., Ohta, K. and Inamura, H.: A Pedestrian Passage Detection Method by using Spinning Magnets on Corridors, *Journal of Information Processing*, Vol.58, No.1, pp.43–56 (2017). (in Japanese).

[22] Takeshima, C., Kaji, K., Hiroi, K., Kawaguchi, N., Kamiyama, T., Ohta, K. and Inamura, H.: A Smartphone Positioning Method based on Spinning Magnet Marker, *Proc. Multimedia, Distributed, Cooperative, and Mobile Symposium* (*DICOMO2016*), pp.889–898 (2016). (in Japanese).

[23] Watanabe, K., Hiroi, K., Kamiyama, S., Sano, H., Tsukamoto, M., Katagiri, M., Ikeda, D., Kaji, K. and Kawaguchi, N.: A Three-Dimensional Smartphone Positioning Method using a Spinning Magnet Marker, *Proc. 2017 10th International Conference on Mobile Computing and Ubiquitous Network* (*ICMU*), pp.1–7 (2017).

Editor's Recommendation

This paper proposes smartphone 3D positioning by using spinning magnet markers. The proposed method has the potential to become one of the key technologies for future positioning devices with the increasing demand for indoor localization and location based services. The method based on the magnetic field change sensed by a smartphone is also beneficial as a reference to signal

processing for other sensors. Therefore, the paper is selected as a recommended paper.

(Chief examiner of SIGMBL Nobuo Kawaguchi)

Kosuke Watanabe received his B.S., M.S. degrees in Science from Tokyo Metropolitan University, Japan, in 2009, 2013, respectively. He received his M.E. degrees in Engineering from Nagoya University, Japan, in 2018. From 2018, he has been a doctoral student in Graduate School of Engneering, Nagoya University, Japan.

Kei Hiroi received her B.S. degree in Engineering in 2004 from Tohoku University. She worked NTT EAST from 2004 to 2011. She received her Master of Media Design and Ph.D. in Media Design in 2011 and 2014, respectively from Keio University. From 2014, she was a designated assistant professor in the Institute of Innovation for Future Society, Nagoya University. Since 2018, she has been an assistant professor in the department Graduate School of Engineering, Nagoya University.

Takeshi Kamiyama joined NTT DOCOMO, INC. in 2006. His research interests include system research, especially energy-efficient design, on mobile device and distributed system. Before NTT DOCOMO, he received M.S. degree in University of Tokyo, Japan in 2006. Also, he was co-founder and CEO in e-jis, Inc. from 2003 to 2006. In 2018, he received Ph.D. degree in Kyushu University, Japan. Currently, He is also a visiting associate professor in Kyushu University. He is a member of IPSJ.

Hiroyuki Sano received his M.S. and Ph.D. degrees in computer science from Nagoya Institute of Technology in 2010 and 2013, respectively. He joined NTT DOCOMO, INC. in 2013. His current research interests include Web intelligence and video analytics. He is a member of IEEE.

Masakatsu Tsukamoto received his Ph.D. degree in information processing from Tokyo Institute of Technology in 2014. He joined NTT DOCOMO, INC. in 2006.

Masaji Katagiri joined Nippon Telegraph and Telephone in 1986. Since 1999, he has been working for NTT DOCOMO. He was a visiting industrial fellow at the University of California at Berkeley from 1990 to 1991, and a lab director of DoCoMo USA Labs from 2002 to 2004. His current research interests include knowledge discovery, social network analysis, and mobile multimedia applications. He received his B. Engineering and M. Engineering degrees from Waseda University, Ph.D. degree from Osaka University, in 1984, 1986 and 2013, respectively. He is a member of IEEE, and IEICE.

Daizo Ikeda received his M.S. degree in technology and policy from Massachusetts Institute of Technology in 2004 and Ph.D. degree from the University of Tokyo in 2013. In 1996, he joined NTT DOCOMO, INC. from 1996 to 2002, he was engaged in development of the packet communication system for i-mode. He has been working on big data analysis for population flow estimation using location data of mobile phones. His research interests include image processing and machine learning. He is a member of IEICE.

Katsuhiko Kaji received his Ph.D. degree in information science from Nagoya University in 2007. He became a RA at NTT Communication Science Laboratories in 2007 and an assistant professor in Nagoya University in 2010. Currently, he is associate professor of Faculty of Information Science, Aichi Institute of Technology from 2015. His research interests include indoor positioning and remote interaction. He is a member of JSSST.

Nobuo Kawaguchi received his B.E, M.E. and Ph.D. degrees in computer science from Nagoya University, Japan, in 1990, 1992, and 1995, respectively. From 1995 he was an associate professor in the department of Electrical and Electronic Engineering and Information Engineering, school of engineering, Nagoya University. Since 2009, he has been a professor in the department of Computational Science and Engineering, graduate school of Engineering, Nagoya University. His research interests are in the areas of human activity recognition, smart environmental system and ubiquitous communication systems.